Strong antiferromagnetic proximity coupling in the heterostructure superconductor math xmlns="http://www.w3.org/1998/Math/MathML">mrow>msub>mi>Sr/mi>mn>2/mn>/msub>msub>mi>VO/mi>mrow>mn>3/mn>mo>−/mo>mi>δ/mi>/mrow>/msub>mi>FeAs/mi>/mrow>/math>

Jong Mok Ok, Chang Il Kwon, O. E. Ayala Valenzuela, Sunghun Kim, Ross D. McDonald, Jeehoon Kim, E. S. Choi, Woun Kang, Y. J. Jo, C. Kim, E. G. Moon, Y. K. Kim, and Jun Sung Kim

Phys. Rev. B **105**, 214505 — Published 6 June 2022

DOI: 10.1103/PhysRevB.105.214505

Strong antiferromagnetic proximity coupling in a heterostructured superconductor $Sr_2VO_{3-\delta}FeAs$

Jong Mok Ok,[1,2,3,*] Chang Il Kwon,[1,2,*] O. E. Ayala Valenzuela,[1] Sunghun Kim,[4] Ross D. McDonald,[5] Jeehoon Kim,[1,2] E. S. Choi,[6] Woun Kang,[7] Y. J. Jo,[8] C. Kim,[9,10] E. G. Moon,[4] Y. K. Kim,[4] and Jun Sung Kim[1,2,†]

[1]*Center for Artificial Low Dimensional Electronic Systems, Institute for Basic Science (IBS), Pohang 37673, Korea*

[2]*Department of Physics, Pohang University of Science and Technology, Pohang 37673, Korea*

[3]*Department of Physics, Pusan National University, Busan 46241, Korea*

[4]*Department of Physics, Korea Advanced Institute of Science and Technology, Daejeon 34141, Korea*

[5]*National High Magnetic Field Laboratory, Los Alamos National Laboratory, Los Alamos, New Mexico 87545, USA*

[6]*National High Magnetic Field Laboratory, Florida State University, Tallahassee, Florida 32310, USA*

[7]*Department of Physics, Ewha Womans University, Seoul 120-750, Korea*

[8]*Department of Physics, Kyungpook National University, Daegu 41566, Korea*

[9]*Department of Physics and Astronomy, Seoul National University, Seoul 08826, Korea*

[10]*Center for Correlated Electron Systems, Institute for Basic Science, Seoul 08826, Korea*

(Dated: May 16, 2022)

Abstract

We report observation of strong magnetic proximity coupling in a heterostructured superconductor $Sr_2VO_{3-\delta}FeAs$, determined by the upper critical fields $H_{c2}(T)$ measurements up to 65 T. Using the resistivity and the radio-frequency measurements for both $H \parallel ab$ and $H \parallel c$, we found a strong upward curvature of $H_{c2}^{c}(T)$, together with a steep increase of $H_{c2}^{ab}(T)$ near T_c, yielding the anisotropic factor $\gamma_H = H_{c2}^{ab}/H_{c2}^{c}$ up to ~ 20, much higher than those of other iron-based superconductors. These are attributed to the Jaccarino-Peter effect, rather than to the multiband effect, due to strong exchange interaction between itinerant Fe spins of the FeAs layers and localized V spins of Mott-insulating $SrVO_{3-\delta}$ layers. These findings provide evidence for strong antiferromagnetic proximity coupling, comparable with the intralayer superexchange interaction of $SrVO_{3-\delta}$ layer and sufficient to induce magnetic frustration in $Sr_2VO_{3-\delta}FeAs$.

Heterostructures of strongly correlated electronic systems offer novel and versatile platforms for triggering various types of exotic electronic orders [1–13]. When one of the constituent layers hosts an itinerant electron system, the other layer in-between serves as an active spacer introducing additional proximity coupling and determines the ground state and the dimensionality of correlated heterostructures. For example, in high-T_c cuprates and iron-based superconductors (FeSCs), the proximity-coupled layers are found to be effective in changing the doping level, modifying the interlayer hopping strength, introducing lattice strain [1–5], or inducing additional pairing interaction by interfacial phonons [6, 7] or charge transfer [8, 9]. Unlike these effects with charge or lattice degrees of freedom, magnetic proximity coupling has often been considered weak and thus playing a secondary role [10–13]. Possible strong magnetic proximity coupling, comparable with the intralayer magentic interaction, may lead to unprecedented electronic phases, which has not been much explored experimentally.

$Sr_2VO_{3-\delta}FeAs$ is a naturally-assembled heterostructure and has a unique position among FeSCs due to possible strong magnetic proximity coupling [14]. In this compound, superconducting FeAs layers and insulating $SrVO_{3-\delta}$ layers are alternately stacked [15, 16] (Fig. 1a), analogous to the superlattice of $FeSe/SrTiO_3$ [17, 18], but with additional magnetic proximity coupling between Fe and V spins. The $SrVO_{3-\delta}$ layers have been identified to be in the Mott-insulating state [16, 19–22], but not to trigger a long-range magnetic transition [16]. Instead, in the FeAs layers, various electronic phase transitions occurs above the superconducting transition at $T_c \sim 30$ K [15, 16, 23], including a mysterious C_4 symmetric transition at $T_0 \sim 150$ K [16, 24–26] without a signature of breaking underlying symmetries [27]. Such a transition has never been observed in other correlated heterostructures, and magnetic proximity coupling that induces frustration between stripe-type Fe and Neel-type V antiferromagnetism, has been suggested as a possible origin [16]. However, whether the magnetic proximity coupling is strong enough, and if so, which type it is, ferromagnetic (FM) or antiferromagnetic (AFM), have remained to be elusive.

In this work, we present experimental evidences for strong AFM exchange coupling of itinerant Fe spins to localized V spins, using the upper critical field H_{c2} of $Sr_2VO_{3-\delta}FeAs$ single crystal for both $H \parallel ab$ and $H \parallel c$, determined by magnetoresistance measurements up to 30 T and radio-frequency (RF) contactless measurements up to 65 T. A strongly convex $H_{c2}^{c}(T)$ for $H \parallel c$ is observed in contrast to a steep linear increase of $H_{c2}^{ab}(T)$ near

T_c for $H \parallel ab$. In comparison with other FeSCs, we found that the Jaccarino-Peter (JP) effect with an exchange field up to $\sim$ 20 T is responsible for this unusual behavior. Our observations confirm that magnetic proximity coupling can play a critical role for inducing unusual magnetic and superconducting properties of $Sr_2VO_{3-\delta}FeAs$.

Single crystals of $Sr_2VO_{3-\delta}FeAs$ were grown using self flux techniques [16]. The typical size of each single crystal was $200\times200\times10$ μm^3. High crystallinity and stoichiometry were confirmed by X-ray diffraction and energy-dispersive spectroscopy. The single crystals show a clear superconducting transition at $T_c^{onset} \sim 27$ K, which is somewhat lower than a maximum $T_c^{onset} \sim 35$ K in a polycrystalline sample [15]. This difference may be attributed to a partial deficiency of oxygen [75]. Magnetotransport measurements were carried out using conventional six-probe method in a 14 T Physical Property Measurement System and a 33 T Bitter magnet at the National High Magnetic Field Lab., Tallahassee. RF contactless measurements up to 65 T were performed in the National High Magnetic Field Lab., Los Alamos.

Before discussing the upper critical field H_{c2} of $Sr_2VO_{3-\delta}FeAs$, we first consider the Fermi surface reconstruction across the C_4 symmetric transition $T_0 \approx 150$ K. According to recent ARPES results on $Sr_2VO_{3-\delta}FeAs$ in the wide range of temperature, the heavy hole FS centered at the Γ point of Brillouin Zone (BZ), denoted h_1 in Figs. 1b and 1c, has a relatively strong k_z dispersion and becomes fully gapped below T_0 [27]. In contrast, the two dimensional electron FS at the M point (e_2 in Figs. 1b and 1c) remains gapless [27]. Concomitantly the additional small electron FS (e_1 in Figs. 1b and 1c), which is absent in the calculated band structures of $Sr_2VO_{3-\delta}FeAs$, is introduced at the Γ point, as illustrated in Figs. 1b and 1c. Because of this unusual band selective gap opening at T_0, low-energy electronic structures of $Sr_2VO_{3-\delta}FeAs$ are significantly reconstructed to yield two separate electron FSs (e_1 and e_2) with strong mismatch in size as shown in Fig. S1 in the Supplemental Materials [28] (see, also, references [76–91] therein). These features are highly distinct from those of other FeSCs. The FS reconstruction of $Sr_2VO_{3-\delta}FeAs$ is also probed by the field dependent Hall resistivity $\rho_{xy}(H)$ of $Sr_2VO_{3-\delta}FeAs$ at different temperatures under magnetic field up to 14 T (Fig. 1d). Above $T_0 \sim 150$ K, a linear field dependence of $\rho_{xy}(H)$ with a negative slope is observed up to $H = 14$ T, similar to the cases of other FeSCs, in which charge conduction is dominated by electron FSs with a high mobility [29]. The contribution of the hole FSs usually appear in $\rho_{xy}(H)$ at low temperatures with a positive slope [28, 30–

35], but is completely absent in $Sr_2VO_{3-\delta}FeAs$.

Instead we found that a non-linear field dependence in $\rho_{xy}(H)$ suddenly appears below T_0, which is well reproduced by the two-band model with two distinct electron carriers. Using a constraint of $1/\rho_{xx}(T) = \sum n_i e\mu_i$, the fit to the two-band model gives us the temperature dependent carrier density (n_i) and carrier mobility (μ_i) as shown in Figs. 1e and 1f. Clearly, additional electron carriers (e_1) with lower density but a higher mobility are induced on top of the high density electron carriers (e_2). The densities of the two electron carriers are estimated to be $\approx 1.1 \times 10^{19}$ cm^{-3} and $\approx 2.3 \times 10^{21}$ cm^{-3}, which are in good agreement with those of the e_1 FS at the Γ ($\approx 2.0 \times 10^{19}$ cm^{-3}) and the e_2 FS at the X point ($\approx 1.1 \times 10^{21}$), obtained by recent ARPES studies [22]. This additional conduction channel of the small FS (e_1) with high mobility compensate for the loss of conduction from the gapped hole FS below T_0, which may explain a weak resistivity anomaly across T_0.

Now we focus on the upper critical field H_{c2} of $Sr_2VO_{3-\delta}FeAs$ single crystals, obtained from the RF measurements and the resistivity (Fig. 2). The radio-frequency curves as a function of magnetic fields along $H \parallel ab$ and $H \parallel c$ yield $H_{c2}(T)$ at various temperatures (Figs. 2a and 2b). Here we determined H_{c2} by taking the magnetic field at which the steepest slope of the radio-frequency intercepts the normal-state background. Temperature and magnetic field dependence of resistivity ρ_{xx} were also used to determine $H_{c2}(T)$ under magnetic field up to 33 T (Supplementary Fig. S2) [28] . Using the criterion of 50% of resistive transition, we obtained $H_{c2}(T)$, consistent with that from the RF contactless measurements. We note that using different criteria for H_{c2} in the RF and the resistivity measurements obtained qualitatively the same $H_{c2}(T)$ behaviour(Supplementary Fig. S3) [28].

Figure 2 (c) shows $H_{c2}(T)$ curves as function of the normalized temperature ($t = T/T_c$) for $H \parallel ab$ and $H \parallel c$. We found that $H_{c2}(T)$ curves taken from different samples and different measurements are consistent with each other. Depending on the magnetic field orientations, $H_{c2}(T)$ exhibits different behaviors. For $H \parallel ab$, $H^{ab}_{c2}(T)$ shows a concave temperature dependence with saturation at low temperatures. This shape is typically observed in many FeSCs [36, 37], in which the Pauli limiting effect dominates over other pair-breaking mechanisms. In contrast, $H^{c}_{c2}(T)$ for $H \parallel c$ shows a strongly convex behaviour with a strong upward curvature. The similar convex behaviours of $H_{c2}(T)$ have been rarely observed, except in some FeSCs including $Ba(Fe,Co)_2As_2$ [38], $(Sr,Eu)(Fe,Co)_2As_2$ [39], LaFeAs(O,F) [40], and NdFeAs(O,F) [41]. However their upward curvature of $H_{c2}(T)$ is far less significant than

found in $Sr_2VO_{3-\delta}FeAs$.

This strong anisotropic behavior of H_{c2} in $Sr_2VO_{3-\delta}FeAs$ can be quantified by the anisotropy factor $\gamma_H = H_{c2}^{ab}/H_{c2}^{c}$. We plot the temperature dependent γ_H for $Sr_2VO_{3-\delta}FeAs$ together with other FeSCs in Fig. 2(d). Near T_c, the slope of $H_{c2}(T)$ is estimated to be $dH_{c2}/dT|_{T_c} \simeq$ -7.4 T/K for $H \parallel ab$ and $\simeq$ -0.2 T/K for $H \parallel c$, in $Sr_2VO_{3-\delta}FeAs$. These make $\gamma_H \sim 20$ at $T \approx T_c$, much higher than those found in FeSCs. As shown in Fig. 2(d), the typical values of γ_H are $\simeq$ 2-3 in the so-called 122 compounds and $\gamma_H \simeq$ 5-6 in the 1111 compounds. Usually, the thicker blocking layer between the superconducting layers induces the stronger anisotropy of H_{c2} with a larger γ_H. The γ_H values of various FeSCs with a different thickness (d) of the blocking layer follow an empirical relation $\gamma_H/d \sim 0.65$ Å^{-1} (Supplementary Fig. S4) [28]. However, $Sr_2VO_{3-\delta}FeAs$ has $\gamma_H \approx 20$, far larger than what is expected, which suggests that the relatively thick blocking layer in $Sr_2VO_{3-\delta}FeAs$ alone cannot explain the observed γ_H and also its strong temperature dependence. Recently, new members of FeCSs, Ca(Fe,Co)AsF [42] and $KCa_2Fe_4As_4F_2$ [43], were found to show a large γ_H near T_c, comparable with that of $Sr_2VO_{3-\delta}FeAs$ near T_c. In these FeSCs, the steep slope of the upper critical field $H_{c2}^{ab}(T)$ for $H \parallel ab$, as compared to the moderate one of $H_{c2}^{c}(T)$ for $H \parallel c$ is responsible for the large γ_H. When the superconductivity approaches to two-dimensional limit, $H_{c2}^{ab}(T) \sim (1 - T/T_c)^{1/2}$ and $H_{c2}^{c}(T) \sim (1 - T/T_c)$ near T_c, leading to a diverging behavior of γ_H near T_c, as nicely demonstrated in $KCa_2Fe_4As_4F_2$[43]. However, in $Sr_2VO_{3-\delta}FeAs$, the large γ_H and its strong temperature dependence are due to the strong upward curvature of $H_{c2}^{c}(T)$ and its low slope near T_c for $H \parallel c$. Thus the temperature dependences of $H_{c2}(T)$ for $H \parallel ab$ and $H \parallel c$ are highly distinct from those of other FeSCs, indicating that the superconducting properties of $Sr_2VO_{3-\delta}FeAs$ is exceptional among FeSCs.

For detailed comparison with other FeSCs, we plot the slopes of the upper critical fields dH_{c2}/dT near T_c for both $H \parallel ab$ and $H \parallel c$ in Fig. 3. In the case of $H \parallel ab$, the normalized slope of the upper critical field at T_c, $-(dH_{c2}^{ab}/dT)/T_c$ is closely related to the diffusivity along the c-axis and thus is sensitive to the interlayer distance. $Sr_2VO_{3-\delta}FeAs$ nicely follows the linear trend of $-(dH_{c2}^{ab}/dT)/T_c$ as a function of the thickness of the blocking layer d (Fig. 3a). The distinct behaviour of $Sr_2VO_{3-\delta}FeAs$ is observed for $H \parallel c$. In the case of $H \parallel c$, $-(dH_{c2}^{c}/dT)/T_c$ is more sensitive to the electronic structure of the FeAs layer than to the interlayer distance. In conventional superconductors, $-(dH_{c2}^{c}/dT)/T_c$ is known to be

proportional to $1/\langle v_F^2 \rangle$ (Fig. 3b, blue dotted-line). The normalized slope $-(dH_{c2}^c/dT)/T_c$ obtained in various FeSCs shows the strong correlation with $1/\langle v_F^2 \rangle$, estimated from the angle resolved photoemission spectroscopy (ARPES) results [22, 54–62] (Fig. 3b). The data for $Sr_2VO_{3-\delta}FeAs$, however, clearly deviate from this trend and show the lowest $-(dH_{c2}^c/dT)/T_c$ value, leading to the largest γ_H among the FeSCs.

For many FeSCs, temperature dependent $H_{c2}^c(T)$ has been understood using the two-band dirty-limit model [63]. In this model, the intra- and inter-band coupling ($\lambda_{11,22}$ and $\lambda_{12,21}$) and diffusivity of each band (D_1, D_2) determines $H_{c2}^c(T)$ (See Supplementary Fig. S5) [28]. The two-band model can also reproduce the strongly convex behavior of $H_{c2}^c(T)$ of $Sr_2VO_{3-\delta}FeAs$, if we assume dominant interband coupling ($\lambda_{11}\lambda_{22} < \lambda_{12}\lambda_{21}$) and an unusually large $\eta = D_1^{ab}/D_2^{ab} \sim 30$ (Supplementary Figs. S5 and S6) [28]. We note however that most of the FeSCs show a concave $H_{c2}^c(T)$, and even in a few cases, like $Ba(Fe,Co)_2As_2$ [38], LaFeAs(O,F) [40] or NdFeAs(O,F) [41], that show a convex $H_{c2}^c(T)$, the highest estimated η is ~ 10 [37], which is far less than the estimate $\eta \sim 30$ for $Sr_2VO_{3-\delta}FeAs$. Furthermore, the hole FS (h_1) centered at the Γ point of BZ is gapped out below T_0 (Figs. 1b and 1c), and therefore cannot participate in the interband superconducting pairing. The remaining interband coupling channel is between electron FSs (e_1 and e_2) centered at Γ and M points (Fig. 1c). However, considering their drastic size difference by two orders of magnitude, confirmed by ARPES and Hall resistivity results, they are unlikely to produce strong interband coupling. These observations suggest that the conventional multiband effect cannot be the origin of the observed $H_{c2}^c(T)$ of $Sr_2VO_{3-\delta}FeAs$.

Instead magnetic coupling between itinerant Fe and localized V spins can offer a natural explanation for a strongly convex behaviour of $H_{c2}^c(T)$. Recent high field magnetoresistance (MR) results reveal a strong negative MR with a clear kink at $\sim$ 38 T for $H \parallel c$, in contrast to the monotonic positive MR for $H \parallel ab$ [27]. These results resemble the case of $EuFe_2As_2$ [64] and indicate a field-induced saturation of magnetic V moment for $H \parallel c$ but not for $H \parallel ab$. Strong exchange coupling J of itinerant Fe electrons to localized V spins is then expected to introduce a net internal magnetic field $H_J = J\langle S \rangle / g_m \mu_B$, which is referred to as the JP effect [65]. With AFM exchange interaction ($J < 0$), a negative H_J is produced by polarization of V spins along the external field, particularly for $H \parallel c$. For paramagnetic V spins, their susceptibility and thus H_J increase with lowering temperatures. Therefore, H_J compensates for the external field and enhances $H_{c2}(T)$ at low temperature with large

external fields. This trend results in a convex $H_{c2}(T)$, as observed in Fig. 2(c).

In the JP model with multiple pair-breaking including the exchange field due to the localized moments [65], $H_{c2}(T)$ can be described as

$$ln\frac{1}{t} = \left(\frac{1}{2} + \frac{i\lambda_{SO}}{4\gamma}\right) \times \Psi\left(\frac{1}{2} + \frac{h + i\lambda_{SO}/2 + i\gamma}{2t}\right) + \left(\frac{1}{2} - \frac{i\lambda_{SO}}{4\gamma}\right) \times \Psi\left(\frac{1}{2} + \frac{h + i\lambda_{SO}/2 - i\gamma}{2t}\right) - \Psi\left(\frac{1}{2}\right), \quad (1)$$

where $\gamma = [\alpha^2(h + h_J)^2 - \lambda_{SO}^2]^{\frac{1}{2}}$, $t = T/T_c$, $h = 0.281H_{c2}/H_{c2}^*$, $h_J = 0.281H_J/H_{c2}^*$, H_{c2}^* is the orbital critical field at T= 0 K, Ψ is the digamma function, λ_{SO} is spin-orbit scattering parameter and α is the Maki parameter [66]. The orbital critical field H_{c2}^* is estimated from the slope $(dH_{c2}/dT)|_{T_c}$ (Fig. 2c) as $H_{c2}^* = -0.69T_c(dH_{c2}/dT)|_{T_c}$, while the typical values of $\alpha = 4$ and $\lambda_{SO} = 0$ are assumed, as widely done for other Fe-based superconductors [67, 68]. Here, the temperature and field dependence of net internal magnetic field $H_J(H, T)$ should follow the susceptibility data of V spins of $Sr_2VO_{3-\delta}FeAs$. As confirmed by the previous V NMR study [16], V local spins remain in the paramagnetic state at low temperatures with a finite antiferromagnetic interaction, of which the strength is estimated by the Curie-Weiss temperature Θ_{CW}= −110 K for $H \parallel c$ and Θ_{CW}= −119 K for $H \parallel ab$ from the magnetic susceptibility [16]. Therefore, the temperature and field dependence of V magnetic moments M follows the Curie-Weiss law, $M(H, T) \propto H/(T-\Theta_{CW})$, and thus $H_J(H, T)$ is described by $H_J(H, T) = \lambda_J M(H, T)$, where λ_J is the factor proportional to the exchange coupling J of itinerant Fe electrons to localized V spins. Using a temperature-independent λ_J as the only fitting parameter, we nicely reproduce the temperature dependent $H_{c2}(T)$ of $Sr_2VO_{3-\delta}FeAs$ for $H \parallel c$ and $H \parallel ab$ as shown in Fig. 4. The coupling constant λ_J and H_J at H_{c2} and zero temperature are listed in Table 1. The good agreement between experiments and calculations strongly suggest that the interlayer coupling between local V spins and itinerant Fe spins can explain the characteristic temperature-dependent $H_{c2}(T)$ of $Sr_2VO_{3-\delta}FeAs$ for $H \parallel c$ and $H \parallel ab$ (Supplementary Fig. S7) [28].

The maximum $H_J \approx$ -22 T of $Sr_2VO_{3-\delta}FeAs$, obtained for $H \parallel c$, is comparable with those of other superconductors, including $EuMo_6S_8$ [69, 70] and λ-(BETS)$FeCl_4$ [71, 72], and far less than $H_J \sim$ -70 T of $EuFe_2As_2$ [64]. The sizable anisotropies in H_J and λ_J are observed between the cases of $H \parallel c$ and $H \parallel ab$ (Table 1). The origin of such anisotropy remains unclear but the similar behaviour has been observed in the case of $EuFe_2As_2$ [64]. For $H \parallel c$, we found that the magnetic interlayer coupling constant $J \sim$ 2.3 meV, estimated from H_J,

is similar in $EuFe_2As_2$ and $Sr_2VO_{3-\delta}FeAs$, considering the smaller $\langle S\rangle = 1$ of V spins with $3d^2$ configurations than $\langle S\rangle = 7/2$ of Eu spins. This observation suggests that they share the similar interlayer coupling between itinerant electrons of the FeAs layers with localized spins in the adjacent layers. Despite the similarity, magnetism of $Sr_2VO_{3-\delta}FeAs$ is highly distinct from that of $EuFe_2As_2$. In $EuFe_2As_2$, Eu magnetism is induced by RKKY interaction due to itinerant Fe electrons [73]. In contrast, the $SrVO_{3-\delta}$ layers in $Sr_2VO_{3-\delta}FeAs$ are in the Mott-insulating state and the localized V spins are coupled through their intralayer superexchange interaction (J_S), competing with the RKKY interaction through the FeAs layers. The interlayer magnetic coupling strength of $J \sim 2.3$ meV in $Sr_2VO_{3-\delta}FeAs$ is comparable with the superexchange interaction of V spins, $J_S \sim 1.6$ meV, estimated from the Curie-Weiss temperature $\Theta_{CW} = -110$ K [16].

The consequences of the strong AFM proximity coupling in $Sr_2VO_{3-\delta}FeAs$ are highly unusual. Without it, the $SrVO_{3-\delta}$ layer in the Mott-insulating state likely hosts the Neel-type AFM order, and the FeAs layer does the stripe-type AFM order. However due to the strong proximity coupling, two inherent magnetic instabilities at each layer are frustrated, which may destabilize these conventional AFM orders in subsystems. The unusual paramagnetism of the V spins, stabilized far below $\Theta_{CW} \sim 100$ K, and the spin gap behaviour of the Fe spins, developed near ~ 200 K [16], are signatures of this magnetic frustration. Furthermore, recent high field transport experiments [27] revealed that the anisotropic magnetoresistance is developed below the mysterious C_4 symmetric transition at $T_0 \sim 150$ K. This indicates spin scattering between itinerant Fe and localized V spins below T_0, consistent with the observed strong magnetic proximity coupling in this work. While the nature and origin of the C_4 symmetric transition at T_0 in $Sr_2VO_{3-\delta}FeAs$ remains to be clarified, these observations highlights the dominant role of magnetic proximity coupling to trigger an exotic electronic order, not present in each subsystem alone. The detailed microscopic understanding on proximity magnetic coupling, particularly its anisotropic nature, is highly desirable.

Our findings on strong magnetic proximity coupling are of considerable relevance in the fields of strongly correlated heterostructures, beyond $Sr_2VO_{3-\delta}FeAs$. The common wisdom states that for the Mott insulating system, additional magnetic coupling across the interface with itinerant electron system is weak and usually leads to a small perturbation on its dominant intralayer magnetic interaction [10–13]. In contrast, $Sr_2VO_{3-\delta}FeAs$ establishes an example that the magnetic proximity coupling competes on an equal footing with the

intralayer magnetic interactions in strongly correlated heterostructures. Our work thus demonstrates that proper design and synthesis on heterostructures of the correlated itinerant and Mott-insulating electron systems can offer a promising material platform studying exotic phases stabilized by frustration of the competing interactions of subsystems and lead to rich physics triggered by dominant magnetic proximity coupling.

ACKNOWLEDGEMENTS

The authors thank Y. G. Bang for fruitful discussion. We also thank H. G. Kim in Pohang Accelerator Laboratory (PAL) for the technical support. This work was supported by the Institute for Basic Science (IBS) through the Center for Artificial Low Dimensional Electronic Systems (no. IBS-R014-D1) and by the National Research Foundation of Korea (NRF) through SRC (Grant No. 2018R1A5A6075964) and the Max Planck-POSTECH Center for Complex Phase Materials (Grant No. 2016K1A4A4A01922028). W.K. acknowledges the support by NRF (No. 2018R1D1A1B07050087, 2018R1A6A1A03025340), and Y.J.J. was supported by NRF (No. NRF-2019R1A2C1089017). J.M.O. acknowledges support from Korea Basic Science Institute (National research Facilities and Equipment Center) grant funded by the Ministry of Education (Grant No. 2021R1A6C101A429) and National Research Foundation of Korea (NRF) grant funded by the Korea government (MSIT) (No. 2021R1F1A1056934). A portion of this work was performed at the National High Magnetic Field Laboratory, which is supported by the National Science Foundation Cooperative Agreement No. DMR-1644779 and the state of Florida.

---

* equal contribution

† Electronic address: `js.kim@postech.ac.kr`

[1] A. Damascelli, Z. Hussain, and Z.-X. Shen, Rev. Mod. Phys. **75**, 473-541 (2003).

[2] J. Chakhalian, J.W. Freeland, G. Srajer, J. Strempfer, G. Khaliullin, J. C. Cezar, T. Charlton, R. Dalgliesh, C. Bernhard, G. Cristiani, H.-U. Habermeier, and B.Keimer, Nat. Phys. **2**, 244248 (2006).

[3] A. Gozar, G. Logvenov, L. Fitting Kourkoutis, A. T. Bollinger, L. A. Giannuzzi, D. A. Muller, and I. Bozovic, Nature **455**, 782785 (2008).

[4] D. K. Satapathy, M. A. Uribe-Laverde, I. Marozau, V. K. Malik, S. Das, Th. Wagner, C. Marcelot, J. Stahn, S. Brck, A. Rhm, S. Macke, T. Tietze, E. Goering, A. Fra, J. -H. Kim, M. Wu, E. Benckiser, B. Keimer, A. Devishvili, B. P. Toperverg, M. Merz, P. Nagel, S. Schuppler, and C. Bernhard, Phys. Rev. Lett. **108**, 197201 (2012).

[5] N. Driza, S. Blanco-Canosa, M. Bakr, S. Soltan, M. Khalid, L. Mustafa, K. Kawashima, G. Christiani, H-U. Habermeier, G. Khaliullin, C. Ulrich, M. Le Tacon, and B. Keimer, Nat. Mater. **11**, 675681 (2012).

[6] J.-F. Ge, Z.-L. Liu, C. Liu, C.-L. Gao, D. Qian, Q.-K. Xue, Y. Liu, and J.-F. Jia, Nat. Mater. **14**, 285 (2015).

[7] J. J. Lee, F. T. Schmitt, R. G. Moore, S. Johnston, Y.-T. Cui, W. Li, M. Yi, Z. K. Liu, M. Hashimoto, Y. Zhang, D. H. Lu, T. P. Devereaux, D.-H. Lee, and Z.-X. Shen, Nature **515**, 245 (2014).

[8] B. Lei, J. H. Cui, Z. J. Xiang, C. Shang, N. Z. Wang, G. J. Ye, X. G. Luo, T. Wu, Z. Sun, and X. H. Chen, Phys. Rev. Lett. **116**, 077002 (2016).

[9] W. S. Kyung, S. S. Huh, Y. Y. Koh, K.-Y. Choi, M. Nakajima, H. Eisaki, J. D. Denlinger, S.-K. Mo, C. Kim, and Y. K. Kim, Nat. Mater **15**, 1233-1236 (2016).

[10] V. Sunko, F. Mazzola, S. Kitamura, S. Khim, P. Kushwaha, O. J. Clark, M. D. Watson, I. Markovi, D. Biswas, L. Pourovskii, T. K. Kim, T.-L. Lee, P. K. Thakur, H. Rosner, A. Georges, R. Moessner, T. Oka, A. P. Mackenzie, and P. D. C. King, Sci. Adv. **6**, 0611 (2020).

[11] J. -H. She, C. H. Kim, C. J. Fennie, M. J. Lawler, and E. -A. Kim, npj Quantum Mater. **2**, 64 (2017).

[12] N. Rohling, E. L. Fjaerbu, and A. Brataas, Phys. Rev. B **97**, 115401 (2018).

[13] E. L. Fjaerbu, N. Rohling, and A. Brataas, Phys. Rev. B **100**, 125432 (2019).

[14] In order to emphasize the naturally-assembled heterostructure, we used the term $Sr_2VO_{3-\delta}FeAs$ rather than $Sr_2VFeAsO_{3-\delta}$ following the international rule. SEe Z. Hiroi, arxiv:0805.4668 (2008).

[15] X. Zhu, F. Han, G. Mu, P. Cheng, B. Shen, B. Zeng, and H.-H. Wen, Phys. Rev. B **79**, 220512(R) (2009).

[16] J. M. Ok, S.-H. Baek, C. Hoch, R. K. Kremer, S. Y. Park, S. Ji, B. Büchner, J.-H. Park, S. I. Hyun, J. H. Shim, Y. Bang, E. G. Moon, I. I. Mazin, and J. S. Kim, Nat. Commun. **8**, 2167 (2017).

[17] S. Choi, S. Johnston, W.-J. Jang, K. Koepernik, K. Nakatsukasa, J. M. Ok, H.-J. Lee, H. W. Choi, A. T. Lee, A. Akbari, Y. K. Semertzidis, Y. Bang, J. S. Kim, and J. Lee, Phys. Rev. Lett. **119**, 107003 (2017).

[18] S. Choi, H. J. Choi, J. M. Ok, Y. Lee, W.-J. Jang, A. T. Lee, Y. Kuk, S. Lee, A. J. Heinrich, S.-W. Cheong, Y. Bang, S. Johnston, J. S. Kim, and J. Lee, Phys. Rev. Lett. **119**, 227001 (2017).

[19] N. H. Nakamura, and M. Machida, Phys. Rev. B **82**, 094503 (2010).

[20] J. M. Ok, S. Na, and J. S. Kim, Prog. Supercond. Cryog. **20**, 28-31 (2018).

[21] T. Qian, N. Xu, Y.-B. Shi, K. Nakayama, P. Richard, T. Kawahara, T. Sato, T. Takahashi, M. Neupane, Y.-M. Xu, X.-P. Wang, G. Xu, X. Dai, Z. Fang, P. Cheng, H.-H. Wen, and H. Ding, Phys. Rev. B **83**, 140513 (2011).

[22] Y. K. Kim, Y. Y. Koh, W. S. Kyung, G. R. Han, B. Lee, Kee Hoon Kim, J. M. Ok, Jun Sung Kim, M. Arita, K. Shimada, H. Namatame, M. Taniguchi, S.-K. Mo, and C. Kim, Phys. Rev. B **92**, 041116 (2015).

[23] G. H. Cao, Z. Ma, C. Wang, Y. Sun, J. Bao, S. Jiang, Y. Luo, C. Feng, Y. Zhou, Z. Xie, F. Hu, S. Wei, I. Nowik, I. Felner, L. Zhang, Z. Xu, and F. C. Zhang, Phys. Rev. B **82**, 104518 (2010).

[24] K. Ueshima, F. Han, X. Zhu, H.-H. Wen, S. Kawasaki, and G. Zheng, Phys. Rev. B **89**, 184506 (2014).

[25] A. S. Sefat, D. J. Singh, V. O. Garlea, Y. L. Zuev, M. A. McGuire, and B. C. Sales, Physica C **471**, 143-149 (2011).

[26] S. Tatematsu, E. Satomi, Y. Kobayashi, and M. Sato, J. Phys. Soc. Jpn. **79**, 123712 (2010).

[27] S. Kim, J. M. Ok, H. Oh, C. Kwon, Y. Zhang, J. D. Denlinger, S. -K. Mo, F. Wolff-Fabrix, E. Kampert, E. Moon, C. Kim, J. S. Kim, and Y. K. Kim, Proc. Natl. Acad. Sci. **118** e2105190118 (2021).

[28] See Supplemental Material [URL will be inserted by publisher] for additional information regarding Hall effect and upper critical fields of $Sr_2VO_{3-\delta}FeAs$ in comparison with other FeSCs.

[29] F. Rullier-Albenque, D. Colson, A. Forget, and H. Alloul, Phys. Rev. Lett. **109**, 187005 (2012).

[30] M. D. Watson, T. Yamashita, S. Kasahara, W. Knafo, M. Nardone, J. Beard, F. Hardy, A. McCollam, A. Narayanan, S. F. Blake, T. Wolf, A. A. Haghighirad, C. Meingast, A. J.

Schofield, H. von Lohneysen, Y. Matsuda, A. I. Coldea, and T. Shibauchi, Phys. Rev. Lett. **115**, 027006 (2015).

[31] S. Ishida, T. Liang, M. Nakajima, K. Kihou, C.H. Lee, A. Iyo, H. Eisaki, T. Kakeshita, T. Kida, M. Hagiwara, Y. Tomioka, T. Ito, and S. Uchida, Phys. Rev. B **84**, 184514 (2011).

[32] X. Xing, W. Zhou, N. Zhou, F. Yuan, Y. Pan, H. Zhao, X. Xu and Z. Shi, Supercond. Sci. Technol. **29**, 055005 (2016).

[33] G. F. Chen, W. Z. Hu, J. L. Luo, and N. L. Wang, Phys. Rev. Lett. **102**, 227004 (2009).

[34] J. P. Peña, M. M. Piva, P. F. S. Rosa, P. G. Pagliuso, C. Adriano, T. Grant, Z. Fisk, E. Baggio-Saitovitch, and P. Pureur, Phys. Rev. B **97**, 104502 (2018).

[35] X. Zhu, H. Yang, L. Fang, G. Mu, and H. H. Wen, Supercond. Sci. Technol. **21**, 105001 (2008).

[36] A. Gurevich, Rep. Prog. Phys. **74**, 124501 (2011).

[37] J. L. Zhang, L. Liao, Y. Chen, and H. Q. Yuan, Front. Phys. **6**(4), 463 (2011).

[38] M. Kano, Y. Kohama, D. Graf, F. Balakirev, A. S. Sefat, M. A. Mcguire, B. C. Sales, D. Mandrus, and S. W. Tozer, J. Phys. Soc. Jpn. **78**, 084719 (2009).

[39] R. Hu, E. D. Mun, M. M. Altarawneh, C. H. Mielke, V. S. Zapf, S. L. Bud'ko, and P. C. Canfield, Phys. Rev. B **85**, 064511 (2012).

[40] F. Hunte, J. Jaroszynski, A. Gurevich, D. C. Larbalestier, R. Jin, A. S. Sefat, M. A. McGuire, B. C. Sales, D. K. Christen, and D. Mandrus, Nature **453**, 903-905 (2008).

[41] J. Jaroszynski, F. Hunte, L. Balicas, Y. Jo, I. Raičević, A. Gurevich, D. C. Larbalestier, F. F. Balakirev, L. Fang, P. Cheng, Y. Jia, and H. H. Wen, Phys. Rev. B **78**, 174523 (2008).

[42] Yonghui Ma, Qiucheng Ji, Kangkang Hu, Bo Gao, Wei Li, Gang Mu, and Xiaoming Xie, Supercond. Sci. Technol. **30**, 074003 (2017).

[43] Teng Wang, Chi Zhang, LiangCai Xu, JinHua Wang, Shan Jiang, ZengWei Zhu, ZhaoSheng Wang, JiaNan Chu, JiaXin Feng, LingLing Wang, Wei Li, Tao Hu, XiaoSong Liu, and Gang Mu, Sci. China-Phys. Mech. Astron. **63**, 227412 (2020)

[44] M. D. Watson, A. McCollam, S. F. Blake, D. Vignolles, L. Drigo, I. I. Mazin, D. Guterding, H. O. Jeschke, R. Valentí, N. Ni, R. Cava, and A. I. Coldea, Phys. Rev. B **89**, 205136 (2014).

[45] E. Mun, N. Ni, J. M. Allred, R. J. Cava, O. Ayala, R. D. McDonald, N. Harrison, and V. S. Zapf, Phys. Rev. B **85**, 100502 (2012).

[46] X. Xing, W. Zhou, J. Wang, Z. Zhu, Y. Zhang, N. Zhou, B. Qian, X. Xu, and Z. Shi, Sci. Rep. **7**, 45943 (2017).

[47] L. Jiao, Y. Kohama, J. L. Zhang, H. D. Wang, B. Maiorov,F. F. Balakirev, Y. Chen, L. N. Wang, T. Shang, M. H. Fang, and H. Q. Yuan, Phys. Rev. B **85**, 064513 (2012).

[48] H.-S. Lee, M. Bartkowiak, J.-H. Park, J.-Y. Lee, J.-Y. Kim, N.-H. Sung, B. K. Cho, C.-U. Jung, J. S. Kim, and H.-J. Lee, Phys. Rev. B **80**, 144512 (2009).

[49] J. M. Ok, C. I. Kwon, Y. Kohama, J. S. You, S. K. Park, J. Kim, Y. J. Jo, E. S. Choi, K. Kindo, W. Kang, K.-S. Kim, E. G. Moon, A. Gurevich, and J. S. Kim, Phys. Rev. B **101**, 224509 (2020).

[50] C. I. Kwon, J. M. Ok, and J. S. Kim, Prog. Supercond. Cryog. **16**, 26-30 (2014).

[51] J. L. Zhang, L. Jiao, F. F. Balakirev, X. C. Wang, C. Q. Jin, and H. Q. Yuan, Phys. Rev. B **83**, 174506 (2011).

[52] J. Xing, B. Shen, B. Zeng, J. Liu, X. Ding, Z. Wang, H. Yang, and H.-H. Wen, Sci. China-Phys. Mech. Astron. **55**, 2259 (2012).

[53] N. Kurita, M. Kimata, K. Kodama, A. Harada, M. Tomita, H. S. Suzuki, T. Matsumoto, K. Murata, S. Uji, and T. Terashima, Phys. Rev. B **88** 224510 (2013).

[54] Z. K. Liu, M. Yi, Y. Zhang, J. Hu, R. Yu, J.-X. Zhu, R.-H. He, Y. L. Chen, M. Hashimoto, R. G. Moore, S.-K. Mo, Z. Hussain, Q. Si, Z. Q. Mao, D. H. Lu, and Z.-X. Shen, Phys. Rev. B **92**, 235138 (2015).

[55] H. Ding, K. Nakayama, P. Richard, S. Souma, T. Sato, T. Takahashi, M. Neupane, Y. M. Xu, Z. H. Pan, A. V. Fedorov, Z. Wang, X. Dai, Z. Fang, G. F. Chen, J. L. Luo, and N. L. Wang, Phys. Condens. Matter **23**, 135701 (2011).

[56] B. Mansart, E. Papalazarou, M. F. Jensen, V. Brouet, L. Petaccia, L. de Medici, G. Sangiovanni, F. Rullier-Albenque, A. Forget, D. Colson, and M. Marsi, Phys. Rev. B **85**, 144508 (2012).

[57] Y. Zhang, J. Wei, H. W. Ou, J. F. Zhao, B. Zhou, F. Chen, M. Xu, C. He, G. Wu, H. Chen, M. Arita, K. Shimada, H. Namatame, M. Taniguchi, X. H. Chen, and D. L. Feng, Phys. Rev. Lett. **102**, 127003 (2009).

[58] S. V. Borisenko, D. V. Evtushinsky, Z.-H. Liu, I. Morozov, R. Kappenberger, S. Wurmehl, B. Buchner, A. N. Yaresko, T. K. Kim, M. Hoesch, T. Wolf, and N. D. Zhigadlo, Nat. Phys. **12**, 311 (2016).

[59] L. X. Yang, B. P. Xie, Y. Zhang, C. He, Q. Q. Ge, X. F. Wang, X. H. Chen, M. Arita, J. Jiang, K. Shimada, M. Taniguchi, I. Vobornik, G. Rossi, J. P. Hu, D. H. Lu, Z. X. Shen, Z.

Y. Lu, and D. L. Feng, Phys. Rev. B **82**, 104519 (2010).

[60] D. H. Lu, M. Yi, S.-K. Mo, A. S. Erickson, J. Analytis, J.-H. Chu, D. J. Singh, Z. Hussain, T. H. Geballe, I. R. Fisher, and Z.-X. Shen, Nature **455**, 81 (2008).

[61] C. Liu, T. Kondo, A. D. Palczewski, G. D. Samolyuk, Y. Lee, M. E. Tillman, N. Ni, E. D. Mun, R. Gordon, A. F. Santander-Syro, S. L. Budko, J. L. McChesney, E. Rotenberg, A. V. Fedorov, T. Valla, O. Copie, M. A. Tanatar, C. Martin, B. N. Harmon, P. C. Canfield, R. Prozorov, J. Schmalian, and A. Kaminski, Physica C **469**, 491 (2009).

[62] S. Jiang, L. Liu, M. Schutt, A. M. Hallas, B. Shen, W. Tian, E. Emmanouilidou, A. Shi, G. M. Luke, Y. J. Uemura, R. M. Fernandes, and N. Ni, Phys. Rev. B **93**, 174513 (2016).

[63] A. Gurevich, Phys. Rev. B **67**, 184515 (2003).

[64] N. Kurita, M. Kimata, K. Kodama, A. Harada, M. Tomita, H. S. Suzuki, T. Matsumoto, K. Murata, S. Uji, and T. Terashima, Phys. Rev. B **83**, 100501(R) (2011).

[65] V. Jaccarino, and M. Peter, Phys. Rev. Lett. **9**, 290 (1962).

[66] K. Maki, Phys. Rev. **148**, 362 (1966).

[67] S. Khim, B. Lee, J. W. Kim, E. S. Choi, G. R. Stewart, and K. H. Kim, Phys. Rev. B **84**, 104502 (2011).

[68] T. Terashima, M. Kimata, H. Satsukawa, A. Harada, K. Hazama, S. Uji, H. Harima, G.-F. Chen, J.-L. Luo, and N.-L. Wang, J. Phys. Soc. Jpn. **78**, 063702 (2009)

[69] M. Decroux, S. E. Lambert, M. S. Torikachvili, M. B. Maple, R. P. Guertin, L. D. Woolf, and R. Baillif, Phys. Rev. Lett. **52**, 1563 (1984).

[70] H. W. Meul, C. Rossel, M. Decroux, O. Fischer, G. Remenyi, and A. Briggs, Phys. Rev. Lett. **53**, 497 (1984).

[71] S. Uji, H. Shinagawa, T. Terashima, T. Yakabe, Y. Terai, M. Tokumoto, A. Kobayashi, H. Tanaka, and H. Kobayashi, Nature (London) **410**, 908 (2001).

[72] K. Hiraki, H. Mayaffre, M. Horvatic, C. Berthier, S. Uji, T. Yamaguchi, H. Tanaka, A. Kobayashi, H. Kobayashi, and T. Takahashi, J. Phys. Soc.Jpn. **76**, 124708 (2007).

[73] S. Zapf, and M. Dressel, Rep. Prog. Phys. **80** 016501 (2017)

[74] I. I. Mazin, Phys. Rev. B **81**, 020507 (2010).

[75] R. C. Che, F. Han, C. Y. Liang, X. B. Zhao, and H. H. Wen, Phys. Rev. B **90**, 104503 (2014).

[76] S. Kasahara, K. Hashimoto, H. Ikeda, T. Terashima, Y. Matsuda, and T. Shibauch, Phys. Rev. B **85**, 060503(R) (2012).

[77] F. Rullier-Albenque, D. Colson, A. Forget, P. Thuery, and S. Poissonnet, Phys. Rev. B **81**, 224503 (2010).

[78] Liam S. Farrar, Matthew Bristow, Amir A. Haghighirad, Alix McCollam, Simon J. Bending, and Amalia I. Coldea,npj Quantum Materials **5**, 29 (2020).

[79] R. X. Cao, Jun Dong, Q. L. Wang, Y. J. Yang, C. Zhao, X. H. Zeng, D. A. Chareev, A. N. Vasiliev, Bing Wu, and Guoqing Wu, AIP Advances **9**, 045220 (2019).

[80] S. Ghannadzadeh, J. D. Wright, F. R. Foronda, S. J. Blundell, S. J. Clarke, and P. A. Goddard, Phys. Rev. B **89**, 054502 (2014).

[81] Soshi Takeshita and Ryosuke Kadono, New J. Phys. **11**, 035006 (2009).

[82] M. Nakajima, S. Ishida, T. Tanaka, K. Kihou, Y. Tomioka, T. Saito, C. H. Lee, H. Fukazawa, Y. Kohori, T. Kakeshita, A. Iyo, T. Ito, H. Eisaki, and S. Uchida, Sci. Rep. **4**, 5873 (2014).

[83] I. Pallecchi, C. Tarantini, Y. Shen, R. K. Singh, N. Newman, P. Cheng, Y. Jia, H.-H. Wen, and M. Putti, Supercond. Sci. Technol. **31**, 034007 (2018).

[84] K. Cho, H. Kim, M. A. Tanatar, Y. J. Song, Y. S. Kwon, W. A. Coniglio, C. C. Agosta, A. Gurevich, and R. Prozorov, Phys. Rev. B **83**, 060502(R) (2011).

[85] D. A. Zocco, K. Grube, F. Eilers, T. Wolf, and H. v. Löhneysen, Phys. Rev. Lett. **111**, 057007 (2013).

[86] Chang-woo Cho, Jonathan Haiwei Yang, Noah F.Q. Yuan, Junying Shen, Thomas Wolf, and Rolf Lortz, Phys. Rev. Lett. **119**, 217002 (2017).

[87] H. Lei, R. Hu, E. S. Choi, J. B. Warren, and C. Petrovic, Phys. Rev. B **81**, 094518 (2010).

[88] S. A. Baily, Y. Kohama, H. Hiramatsu, B. Maiorov, F. F. Balakirev, M. Hirano, and H. Hosono, Phys. Rev. Lett. **102**, 117004 (2009).

[89] M. Fang, J. Yang, F. F. Balakirev, Y. Kohama, J. Singleton, B. Qian, Z. Q. Mao, H. Wang, and H. Q. Yuan, Phys. Rev. B **81**, 020509(R) (2010).

[90] S. K. Goh, Y. Nakai, K. Ishida, L. E. Klintberg, Y. Ihara, S. Kasahara, T. Shibauchi, Y. Matsuda, and T. Terashima, Phys. Rev. B **82**, 094502 (2010).

[91] L. Jiao, J.L. Zhang, F.F. Balakirev, G.F. Chen, J.L. Luo, N.L. Wang, H.Q. Yuan, J. Phys. Chem. Solids **72**, 423-425 (2011).

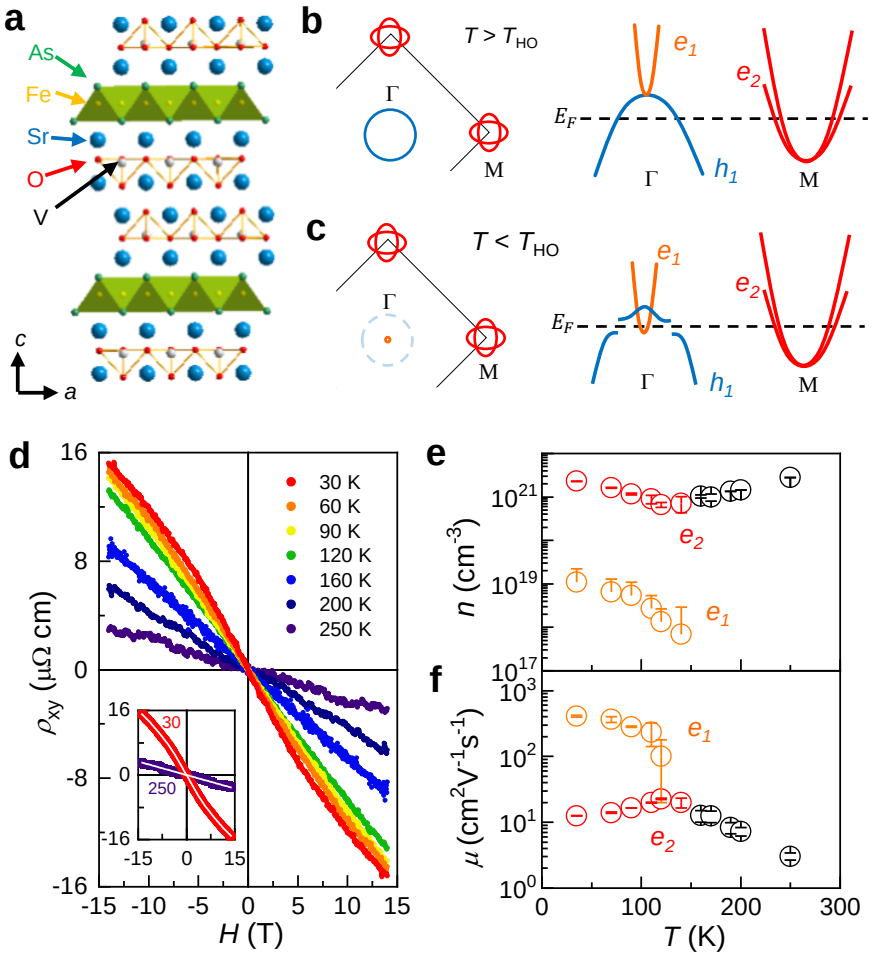

FIG. 1: (a) Crystal structure of $Sr_2VO_{3-\delta}FeAs$ consisting of FeAs layers and $SrVO_{3-\delta}$ layers. Schematic illustration of Fermi surface and band structures above (b) and below (c) $T_0 = 150$ K. (d) Magnetic field dependence of the Hall resistivity $\rho_{xy}(H)$ measured at different temperatures. The white solid lines in the inset represent best fits for Hall data. Temperature dependence of the carrier density (e) and the mobility (f), extracted from the fits using one band model (black) for $T > T_0$ and two-band model (red and orange) for $T < T_0$.

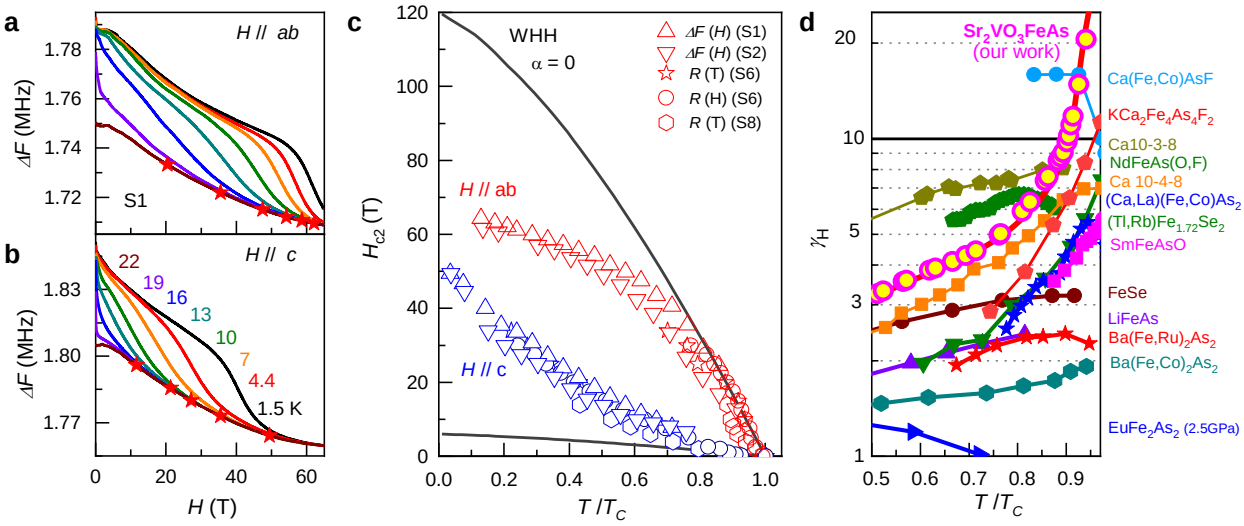

FIG. 2: Magnetic field dependence of the radio-frequency for (a) $H \parallel ab$ and (b) $H \parallel c$. Red stars show estimated H_{c2}. (c) Upper critical field $H_{c2}(T)$ for $H \parallel ab$ (red open symbols) and $H \parallel c$ (blue open symbols) as a function of the normalized temperature T/T_c for the four crystals (S1, S2, S6, S8) estimated from the tunnel diode oscillator and resistivity measurements. Black solid lines are Werthamer-Helfand-Hohenberg curves with $\alpha = 0$. (d) Temperature dependent anisotropic factor γ_H of $Sr_2VO_{3-\delta}FeAs$ and other FeSCs [38, 41, 44–53]. Red solid line shows γ_H of $Sr_2VO_{3-\delta}FeAs$ calculated from the $H_{c2}(T)$ fits for comparison.

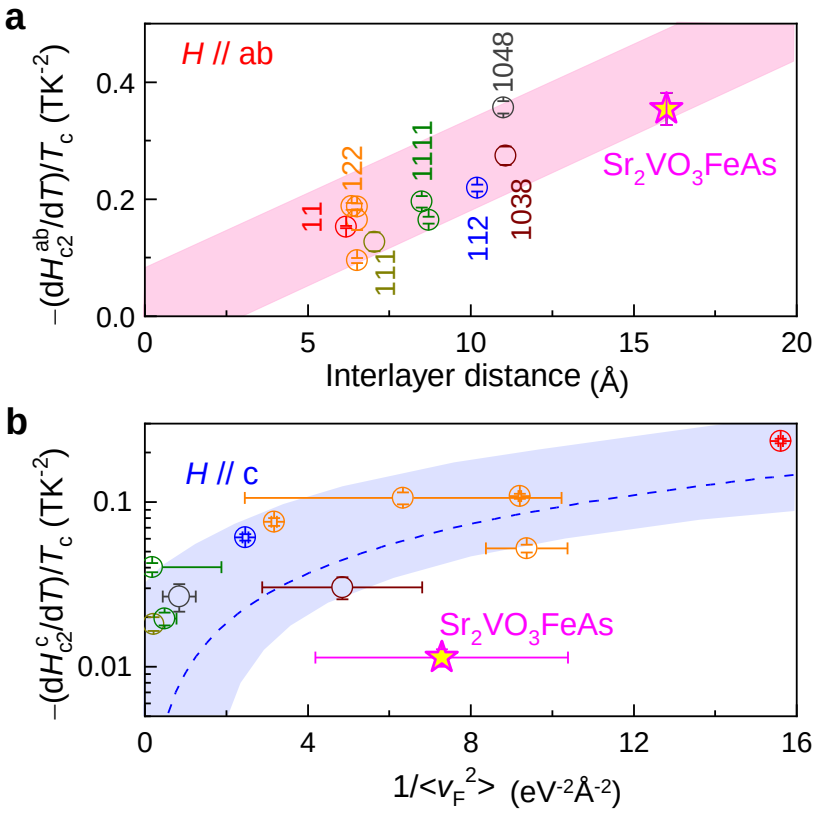

FIG. 3: (a) Interlayer distance dependence of normalized slope of $H_{c2}(T)$ near T_c for $H \parallel ab$. The normalized slope of $H_{c2}(T)$ increases in proportion to the interlayer distance. (b) Normalized slope of $H_{c2}(T)$ near T_c for $H \parallel c$ as a function of $< v_F^2 >$, which are estimated from ARPES results [22, 54–62].

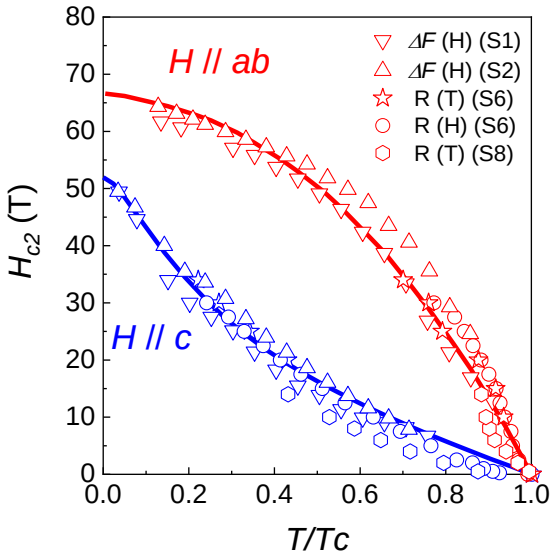

FIG. 4: Temperature dependent upper critical field $H_{c2}(T)$ of $Sr_2VO_{3-\delta}FeAs$ for both $H \parallel ab$ and $H \parallel c$. Red and blue solid lines are Jaccarino-Peter fits for $H \parallel ab$ and $H \parallel c$, respectively.

TABLE I: Maximum H_J and λ_J of $Sr_2VO_{3-\delta}FeAs$ for both directions compared to other materials.

	T_c [K]	$\lvert H_J^{ab}\rvert$ [T]	$\lvert H_J^{c}\rvert$ [T]	$\lvert \lambda_J^{ab}\rvert$	$\lvert \lambda_J^{c}\rvert$
Sr_2VO_3FeAs	30	19.5	22.3	141	204
$EuFe_2As_2$ [64]	30	168	70	187	83
$EuMo_6S_6$ [69, 70]	12		38		383
λ-(BETS)$FeCl_4$ [71, 72]	4.2		32		813